Integration of Crack-Tolerant Composite Gridlines on Triple Junction Photovoltaic Cells

Omar K. Abudayyeh[1], Geoffrey K. Bradshaw[2], *Member*, *IEEE*, Steven Whipple[3], David M. Wilt[2], and Sang M. Han[1]

[1]University of New Mexico, Albuquerque, NM, 87131, USA
[2]Air Force Research Laboratory, KAFB, NM, 87123
[3]SolAero Technologies, Albuquerque, NM, 87123

***Abstract*—Metal matrix composites consisting of multi-walled carbon nanotubes embedded in a sliver matrix are successfully integrated onto commercial triple junction photovoltaic cells. The performance of triple junction cells with composite gridlines is analyzed; the fill factor and efficiency closely match those of cells with standard evaporation-based metallization. The cells are then intentionally cracked, using external mechanical stress. We observe substantially enhanced crack tolerance in composite-enhanced cells in comparison to standard triple junction cells. Upon introducing cracks, the control cell result in a loss of 54% in the short circuit current, whereas no significant loss is observed for the composite-enhanced cells. The composite metal gridlines show strong potential to improve the lifetime of space photovoltaic cells against stress-induced fracture.**

***Index Terms*—Carbon nanotubes, composite materials, cracking, metallization, photovoltaic cells, reliability, solar cells.**

I. Introduction

Multi-junction (MJ) solar cells have been used almost exclusively for space vehicles due to their high efficiency [1] and high radiation hardness [2]. The efficiency of state-of-practice (SOP) space triple-junction (TJ) cells today are approximately 30% under 1-sun Air Mass 0 (AM0) spectrum [3]. While MJ cells provide a high efficiency, microcracks can develop in crystalline photovoltaic (PV) cells due to a variety of reasons: e.g., growth defects, film stress by lattice mismatch, and mechanical stress introduced during shipping, installation, and operation. Microcracks can electrically isolate fractured portions of the cell, which can lead to a substantial power loss.

To mitigate the performance degradation due to microcracks, we have investigated the use of multi-walled carbon nanotubes (MWCNTs) as mechanical reinforcement to metal gridlines, where CNTs are embedded in the metal to form metal matrix composites (MMC). Our previous work [4] has shown that MMC gridlines (1-mm wide, 6-μm-thick) can electrically bridge > 40-μm-wide fractures and repeatedly "self-heal" when the lines are strained to failure and brought back to close proximity. Fig. 1 shows SEM micrographs of fractured MMC gridlines (~9-μm-wide gap) with MWCNTs bridging the gap while providing redundant electrical conduction pathways.

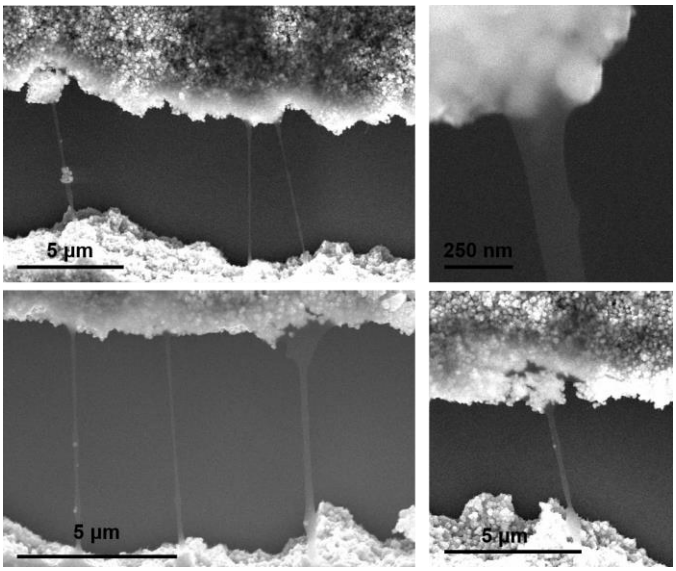

Fig. 1. SEM micrographs of CNTs anchored in Ag layers, bridging 9-μm-wide gaps [4].

The CNTs are deposited on a layer of electrodeposited silver (Ag), and a second layer of Ag is electrodeposited on top of the CNT layer, forming a layer-by-layer microstructure of the MMCs. The MMC gridlines are then integrated onto commercial TJ cells and later fractured to assess the ability of MMC to maintain electrical conductivity. After cracks are introduced, we observe that the cells with MMC gridlines exhibit higher performance than the cells with standard metallization.

II. Experimental Methods

A. Materials

Two sets of 2 cm x 2 cm TJ cells with a modified metallization pattern were used to produce control and MMC-enhanced devices. The gridline width and the front contact pad size are made larger than production cells in order to facilitate MMC integration and testing. Cyanide-free alkaline silver plating solution (E-Brite 50/50 RTP, *Electrochemical Products Inc.*) is used for Ag plating. Low-cost, dry MWCNTs purchased from *SWeNT* are functionalized and suspended in water. For a

more detailed description on CNT solution preparation and Ag plating optimization, refer to Ref. [4]. The CNTs are spray-coated on top of the plated Ag, and another layer of Ag is electroplated on top of the CNT layer. A full description of the CNT deposition method can be found in Ref.[5].

Following the gridline deposition, the cells are characterized through light current-voltage (*LIV*) sweeps and electroluminescence (EL) measurements. An X-25 solar simulator (Mark II, *Spectrolab Inc.*) is used to perform the *LIV* sweeps. The beam is first calibrated using a standard TJ cell, and values are reported under AM0 spectrum. EL measurements are performed by forward biasing the cells at 30 mA (~ 7.5 mA/cm^2). The top subcell (GaInP) strongly emits in the visible region (λ = 683 nm) [6] when forward-biased and can be easily examined with the naked eye to visually locate cracks in the substrate.

B. Silver Plating

Silver can be deposited through a variety of techniques, including screen printing, electro and electroless deposition, and vacuum deposition techniques (e.g., chemical/physical vapor deposition and ion sputtering). Electroplating was chosen as the method of deposition because it is a simple and inexpensive technique capable of producing homogenous, highly reflective, thin-film Ag deposits. Metal electroplating is a process that coats conductive or semi-conductive objects with a thin metal film. The process uses an electrical current to reduce cations of a desired metal from a solution. The process is stable and suitable for growth of thin films and/or nanostructures with potentially enhanced thermoelectrical properties [7, 8].

In our previous work [4, 9], we were able to determine a window of operation for depositing smooth, coherent, and compact silver films in a range of current densities using the aforementioned Ag plating solution. We further optimize the previously developed recipe to plate Ag into the 50-µm-wide, 7-µm-deep recess patterns defined for gridlines. Through careful and systematic manipulation of deposition rates (operating current density), we are able to reproduce high-quality silver gridlines. The first Ag layer is deposited using a two-step process, starting with a slow deposition rate (low current density) for a short period followed by a high deposition rate (ramping up the current density). Ag is plated at -1.7 mA/cm^2 for 400 s followed by -6.7 mA/cm^2 for 800 s, resulting in a 2 to 3-µm-thick Ag film (Fig. 2A). The initial deposition at a low current density creates Ag nucleation sites on the seed layer. The proper formation of these nucleation sites allows for the second-stage growth of uniform Ag layers at a high deposition rate. Without the proper formation of initial nucleation sites, dendrites start to form (Fig. 2B) with coarse surface morphology. The high growth rate corresponds to fast reduction of Ag ions at the surface owing to high charge density. A similar behavior is reported in the literature [10-12]. Yasnikov *et al.* [11] reported the formation of various microstructures (e.g., pentagonal, regular shaped, planar, and dendritic) under different potentiostatic conditions as the overpotential increased from 160 to 200 mV. The formation of such dendrites occurs as a result of severe depletion of silver ions near the cathode.

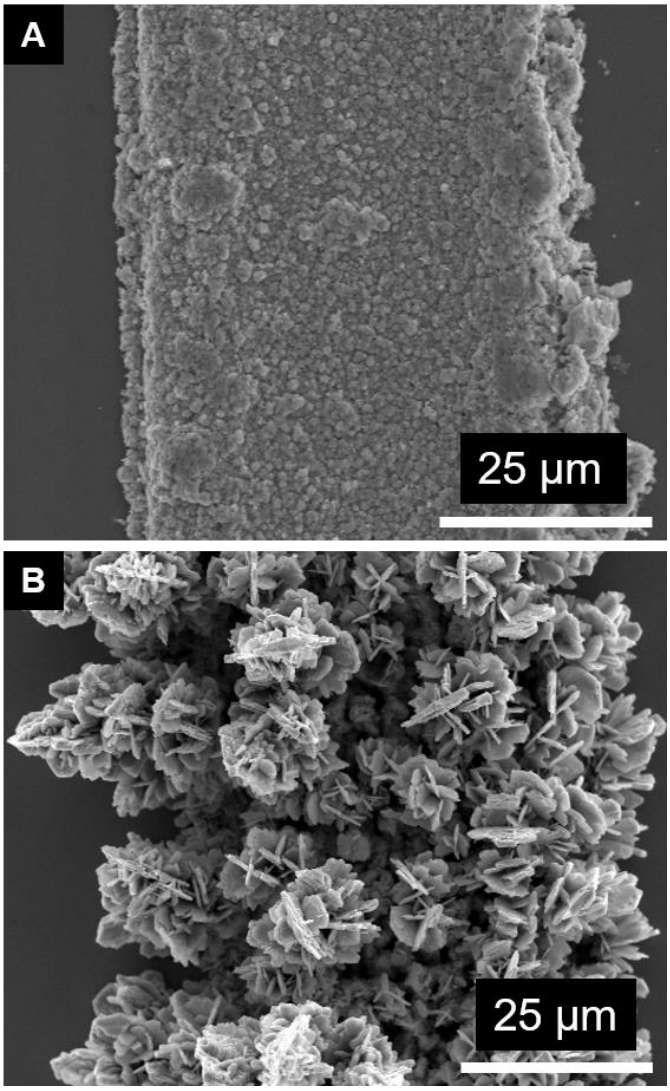

Fig. 2. SEM micrograph (top view) of a gridline after Ag deposition at (A) -1.7 mA/cm^2 for 400 s followed by -6.7 mA/cm^2 for 800 s, resulting in a smooth, dendrite-free gridline; and (B) -6.7 mA/cm^2 for 1200 s, where dendrites form on top of the seed layer creating "desert rose" structures.

C. MMC Integration on TJ Cells

Following the first electroplated Ag layer on TJ cells, the entire cell is spray-coated with an aqueous CNT solution (1.3g/L). The cells are placed on a moving stage (3.5 mm/s) and sprayed 15 times in a repeat cycle, resulting in complete surface coverage of CNTs on Ag. By controlling the moving speed of the sample stage under the spray nozzle and the substrate temperature, we are able to deposit thin, uniform layers of CNTs across the entire surface of the cell. The solvent evaporates quickly from the heated substrate, leaving behind functionalized MWCNTs. The cells are then transferred back into the electrolytic solution for the final deposition of Ag. The second Ag layer is electroplated at -6.7 mA/cm^2 for 500 s, resulting in a ~ 1-µm-thick layer. A short plating time for the second layer is chosen in order to selectively deposit Ag mostly on the gridline pattern and not on the photoresist covered with conductive CNTs. Samples are then rinsed with water to

remove residual plating solution and soaked in acetone to remove the photoresist and CNTs on its top by liftoff.

To verify integration of CNTs within the metal matrix and their homogenous dispersion without agglomeration, the MMC gridlines are examined by scanning electron microscopy (SEM) using a *Hitachi S-4300* at 20 KeV. Figure 3 shows a cross sectional-view of two MMC gridlines. These images show that we can deposit thick (~15-µm) as well as thin (~ 6-µm) gridlines by adjusting the deposition time. CNTs can be seen in the enlarged SEM view (Fig. 3, red arrows) as veiny threads. The CNTs are localized within the stack at a specified depth and appear to adhere well to the surrounding metal matrix. We do not observe agglomeration or bundling of CNTs within the stack; CNTs are well dispersed due to surface functionalization.

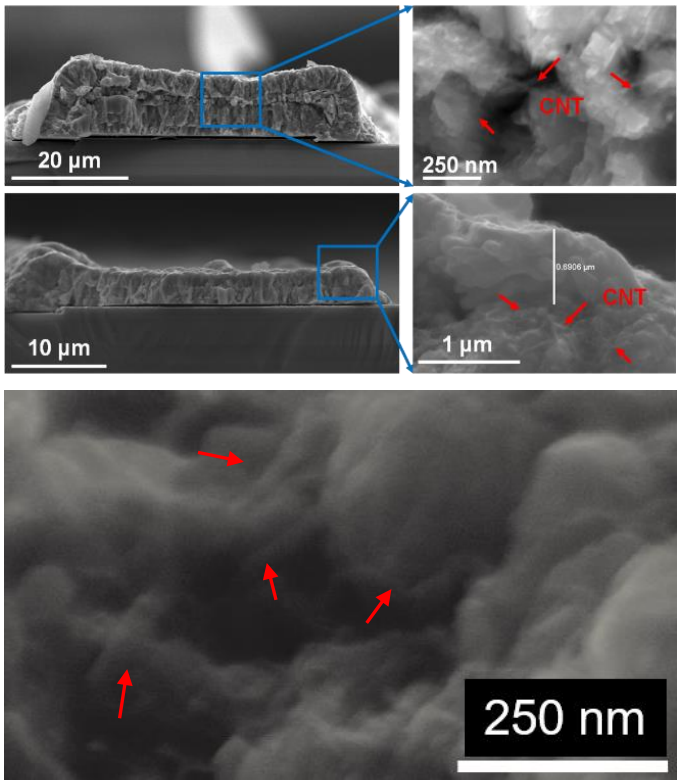

Fig. 3. Cross-sectional SEM micrographs of MMC gridlines on TJ cells. CNTs indicated by red arrows.

III. Results and Discussion

A. MMC Integration

A TJ control sample with standard metallization is used as a baseline for comparing *LIV*, *DIV* and EL characteristics to cells with MMC gridlines. Fig. 4A shows the summary of *LIV* data and EL images of the control sample and five test cells (MMC 1 – 5). The initial attempts of integration resulted in poor cell performance (Fig. 4A, MMC 1 – 3). However, the integration process is later optimized by modifying the electroplating step which resulted in significant improvement in cell performance (Fig. 4A, MMC 4 and 5). The most significant improvement is seen in the *FF* and η reaching 86% and 26%, respectively. Early electroplating attempts resulted in the etching of the cell edges, which can be seen in the EL images of MMC 1 – 3 (Fig. 4A inset), where a non-uniform EL response is observed around the cell edges. This is a result of the plating solution used, which is alkaline with a trace amount of KOH and is a known etchant for most III-V materials [13, 14]. The electroplating step is optimized by properly sealing the cell edges with photoresist prior to electroplating. The dark spots observed are due to KOH etching of the exposed semiconductor material. In comparison, a MMC-integrated TJ cell whose edges are properly sealed during Ag plating (MMC 5 in Fig. 4A) shows a uniform EL response without any dark spots. The result from MMC 5 closely matches the control sample.

To confirm successful integration of MMC gridlines, we examine the diode properties through *DIV* measurements. The inset of Fig. 4B shows the dark diode characteristics of the MMC samples, plotted on semi-log scale. The *DIV* characteristics improve going from MMC 1 to MMC 5 as is particularly evident by the reduced ideality factor at higher voltages. Above 1.5 V, MMC 4 and 5 samples show the diode ideality factor similar to the control sample. For the applied voltage below 1.5 V, the performance of MMC 4 and 5 cells appears to deviate from the control cell. This may be attributed

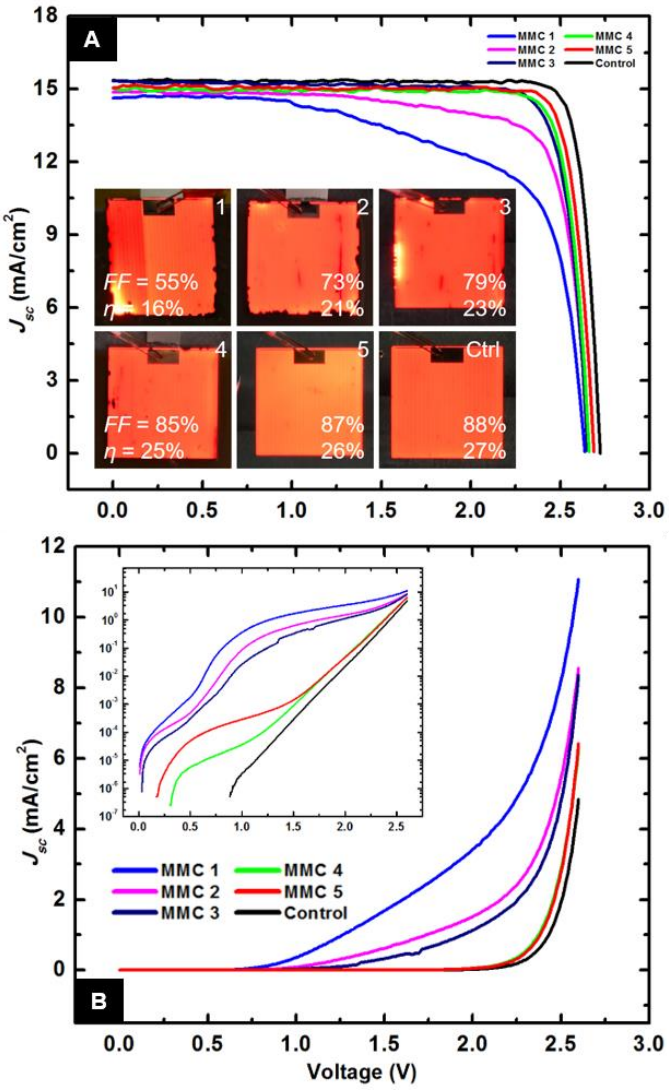

Fig. 4. (A) *LIV* characteristics with EL images of control and 5 MMC test cells, (B) *DIV* scans on linear scale and semi-log scale (inset).

to a small decrease in the shunt resistance of the cells, most likely the result of processing and handling, although the overall cell performance of MMC 4 and 5 is very close to the control sample (Fig. 4A) without any noticeable slope in the current response. In contrast, MMC 1 – 3 samples exhibit poor diode characteristics with a pronounced deviation from the control sample. The non-ideal diode characteristics of MMC 1 – 3 cells are consistent with the poor *LIV* performance, which is largely due to the non-radiative recombination on the exposed areas of the cells that are etched away during Ag deposition.

B. Cell Performance Degradation due to Microcracks

We evaluate the effects of microcracks on the performance of typical TJ cells with standard metallization vs. TJ cell with MMC gridlines. The gridlines on the control cell consist of 100% evaporated Ag, where no CNTs are embedded. *LIV* scan is performed before and after cracking. Cracks are generated by resting cells against a curved surface (r = 6 cm) while applying an external mechanical stress on the cell's top surface. Fig. 5 summarizes the *LIV* and EL results of both control and test samples.

The EL response of the control sample shows a large dark region after introducing cracks. This dark region is the result of electrical isolation from the busbar, where the cracks propagated through both semiconductor and metal gridlines. The illuminated regions correspond to the remaining active cell area that contributes to current generation in the *LIV* scan (Fig. 5). The control sample suffered a significant loss in all cell parameters. A degradation in both V_{oc} (5.1%) and J_{sc} (53%) is clearly observed, demonstrating a possible outcome of cell cracking with Ag gridlines. The *FF* and η also decreased by 29% and 68%, respectively due to cracking. In addition, we note a decrease in shunt resistance and an increase in series resistance of the control cell as a result of cracking.

In contrast, the test sample with MMC gridlines is capable of maintaining electrical continuity even in the presence of cracks. The test cell with MMC gridlines generates nearly the same J_{sc} (0.78% loss) after being fractured. Additionally, the test sample is able to maintain a good EL response after fracturing without any visible dark spots. While both gridlines and substrate are completely fractured, the CNTs appear to provide redundant electrical conduction pathways.

While J_{sc} remains virtually unchanged, we observe brighter EL intensity at and around the fracture locations than the regions that remain intact. The increased brightness suggests an increased number of recombination sites for minority carriers at and around the fracture location. These recombination sites would reduce V_{oc}, as clearly shown in Fig. 5 for both control (5.1% loss) and MMC test (6.1% loss) samples. The V_{oc} loss observed is attributed to the fracturing process and not due to the MMC gridline integration. In addition, the series resistance of the cell with MMC gridlines appears to increase after fracturing. As the gridlines get severed due to microcracks developing in the underlying substrate, the electrical connection in that region is sustained only through the embedded CNTs. Thus, an overall increase in series resistance is observed. This increase in the series resistance ultimately reduces the *FF* and η by 26% and 35%, respectively.

Although the MMC integration on cells may not mitigate against all the loss mechanisms due to fracturing, the test sample with MMC gridlines maintains the same current generation after fracturing. Current preservation is critically important as cells are connected in series on a string, and current loss in one cell can decrease the overall module output.

IV. Conclusion

In this study, we demonstrate the successful integration of MMC gridlines onto commercial TJ cells. These composite lines show strong potential to replace conventional metal ones on space photovoltaic cells. Upon fracturing, the test cells integrated with our MMC gridlines show clearly increased fracture tolerance than the control cell with evaporated Ag gridlines. That is, embedding CNTs into metal mitigates the

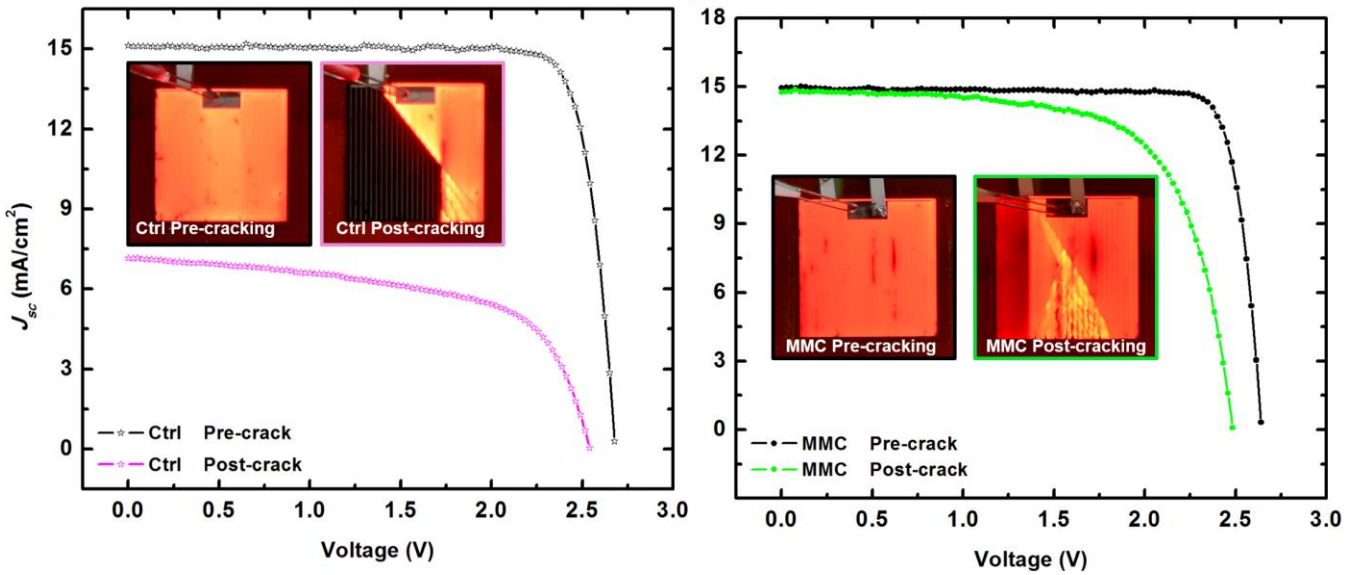

Fig. 5. *LIV* and EL measurement of control (left) composed of bare Ag gridlines, and test sample (right) composed of MMC gridlines.

electrical disconnect due to microcracks. The continuous areal EL response and the preservation of J_{sc} after substrate fracture are strong evidences that MMC lines are more resilient to microcracks developed in the semiconductor substrate than 100% metal gridlines. However, we acknowledge that the cracks may introduce other loss mechanisms that MMCs cannot fully counter, leading to an unavoidable loss in V_{oc}, *FF*, and η. This demonstration supports that our MMC gridlines are suitable to replace traditional gridlines and to help mitigate the loss in cell performance as microcracks develop in cells.

ACKNOWLEDGMENT

We acknowledge a generous financial support from the Air Force Research Laboratory (FA9453-14-1-0242) to conduct this engineering research.

REFERENCES

[1] M. Stan, D. Aiken, B. Cho, A. Cornfeld, J. Diaz, V. Ley, *et al.*, "Very high efficiency triple junction solar cells grown by MOVPE," *Journal of Crystal Growth*, vol. 310, pp. 5204-5208, Nov 2008.

[2] N. Dharmarasu, M. Yamaguchi, A. Khan, T. Yamada, T. Tanabe, S. Takagishi, *et al.*, "High-radiation-resistant InGaP, InGaAsP, and InGaAs solar cells for multijuction solar cells," *Applied Physics Letters*, vol. 79, pp. 2399-2401, Oct 2001.

[3] D. C. Law, J. C. Boisvert, E. M. Rehder, P. T. Chiu, S. Mesropian, R. L. Woo, *et al.*, "Recent Progress of Spectrolab High-Efficiency Space Solar Cells," in *Nanophotonics and Macrophotonics for Space Environments Vii*. vol. 8876, E. W. Taylor and D. A. Cardimona, Eds., ed Bellingham: Spie-Int Soc Optical Engineering, 2013.

[4] O. K. Abudayyeh, N. D. Gapp, C. Nelson, D. M. Wilt, and S. M. Han, "Silver-Carbon-Nanotube Metal Matrix Composites for Metal Contacts on Space Photovoltaic Cells," *IEEE Journal of Photovoltaics*, vol. 6, pp. 337-342, 2016.

[5] O. K. Abudayyeh, N. D. Gapp, G. K. Bradshaw, D. M. Wilt, and S. M. Han, "Spray-coated carbon-nanotubes for crack-tolerant metal matrix composites as photovoltaic gridlines," in *2016 IEEE 43rd Photovoltaic Specialists Conference (PVSC)*, 2016, pp. 0835-0839.

[6] L. J. Kong, Z. M. Wu, S. S. Chen, Y. Y. Cao, Y. Zhang, H. Li, *et al.*, "Performance evaluation of multi-junction solar cells by spatially resolved electroluminescence microscopy," *Nanoscale Research Letters*, vol. 10, pp. 1-7, Feb 2015.

[7] Q. Y. Feng, T. J. Li, Z. T. Zhang, J. Zhang, M. Liu, and J. Z. Jin, "Preparation of nanostructured Ni/Al2O3 composite coatings in high magnetic field," *Surface & Coatings Technology*, vol. 201, pp. 6247-6252, Apr 2007.

[8] N. V. Dziomkina, M. A. Hempenius, and G. J. Vancso, "Towards true 3-dimensional BCC colloidal crystals with controlled lattice orientation," *Polymer*, vol. 50, pp. 5713-5719, 2009.

[9] O. K. Abudayyeh, C. Nelson, S. M. Han, N. Gapp, and D. M. Wilt, "Silver-carbon-nanotube metal matrix composites for metal contacts on space photovoltaic cells," in *2015 IEEE 42nd Photovoltaic Specialist Conference (PVSC)*, 2015, pp. 1-3.

[10] J. X. Fang, H. Hahn, R. Krupke, F. Schramm, T. Scherer, B. J. Ding, *et al.*, "Silver nanowires growth via branch fragmentation of electrochemically grown silver dendrites," *Chemical Communications*, pp. 1130-1132, 2009.

[11] I. S. Yasnikov, Y. D. Gamburg, and P. E. Prokhorov, "Peculiarities of morphology of silver microcrystals electroplated under potentiostatic conditions from ammonium solutions," *Russian Journal of Electrochemistry*, vol. 46, pp. 524-529, May 2010.

[12] Y. H. Cheng and S. Y. Cheng, "Nanostructures formed by Ag nanowires," *Nanotechnology*, vol. 15, pp. 171-175, Jan 2004.

[13] J. R. Mileham, S. J. Pearton, C. R. Abernathy, J. D. MacKenzie, R. J. Shul, and S. P. Kilcoyne, "Patterning of AlN, InN, and GaN in KOH-based solutions," *Journal of Vacuum Science & Technology a-Vacuum Surfaces and Films*, vol. 14, pp. 836-839, May-Jun 1996.

[14] C. Youtsey, I. Adesida, and G. Bulman, "Highly anisotropic photoenhanced wet etching of n-type GaN," *Applied Physics Letters*, vol. 71, pp. 2151-2153, Oct 1997.